Manuscript prepared for Atmos. Chem. Phys.
with version 2015/04/24 7.83 Copernicus papers of the LaTeX class copernicus.cls.
Date: 18 May 2016

Limitations of passive remote sensing to constrain global cloud condensation nuclei

P. Stier

Atmospheric, Oceanic and Planetary Physics, Department of Physics, University of Oxford, Oxford, UK

Correspondence to: P. Stier (philip.stier@physics.ox.ac.uk)

Abstract. Aerosol–cloud interactions are considered a key uncertainty in our understanding of climate change (Boucher et al., 2013). Knowledge of the global abundance of cloud condensation nuclei (CCN) is fundamental to determine the strength of the anthropogenic climate perturbation. Direct measurements are limited and sample only a very small fraction of the globe so that remote sensing from satellites and ground based instruments is widely used as a proxy for cloud condensation nuclei (Nakajima et al., 2001; Andreae, 2009; Clarke and Kapustin, 2010; Boucher et al., 2013). However, the underlying assumptions cannot be robustly tested with the small number of measurements available so that no reliable global estimate of cloud condensation nuclei exists. This study overcomes this limitation using a self-consistent global model (ECHAM-HAM) of aerosol radiative properties and cloud condensation nuclei. An analysis of the correlation of simulated aerosol radiative properties and cloud condensation nuclei reveals that common assumptions about their relationships are violated for a significant fraction of the globe: 71 % of the area of the globe shows correlation coefficients between $CCN_{0.2\%}$ at cloud base and aerosol optical depth (AOD) below 0.5, i.e. AOD variability explains only 25 % of the CCN variance. This has significant implications for satellite based studies of aerosol–cloud interactions. The findings also suggest that vertically resolved remote sensing techniques, such as satellite-based high spectral resolution lidars, have a large potential for global monitoring of cloud condensation nuclei.

1 Introduction

Aerosol–cloud interactions play an important role in the global climate system through modification of aerosol and cloud properties and abundance (Boucher et al., 2013; Twomey, 1974; Albrecht, 1989; Lohmann and Feichter, 2005). The activation of suitable aerosols (cloud condensation nuclei, CCN) to cloud droplets is the primary aerosol effect on warm clouds (and ice or mixed-phase clouds initiated from the liquid phase). Knowledge of the global abundance of aerosols suitable to act as cloud condensation nuclei is fundamental to determine the strength of the anthropogenic perturbation causing the radiative effect of aerosol–cloud interactions. Most estimates of the effect of aerosol–cloud interactions on the global radiation balance rely on global aerosol models. However, large uncertainties associated with the representation of clouds and aerosol effects on cloud microphysics and dynamics in current climate models (Boucher et al., 2013; Stevens and Feingold, 2009) demand for independent observational constraints. Unfortunately, direct observations of CCN are spatio-temporally sparse (Andreae, 2009; Spracklen et al., 2011) and provide insufficient constraints on their global distribution. Consequently, satellite retrieved aerosol radiative properties, such as aerosol optical depth (AOD), have been widely used as proxy for CCN in satellite based studies of aerosol–cloud interactions (Kaufman and Nakajima, 1993; Kaufman et al., 2005; Rosenfeld et al., 2008; Grandey and Stier, 2010; Boucher et al., 2013; Gryspeerdt et al., 2014).

Assuming identical size, shape, composition and humidity, CCN concentrations at fixed supersaturation are linearly related to aerosol light extinction, so that AOD, the column integrated aerosol extinction, could be expected to provide a first order proxy for CCN. However, for realistic aerosol distributions extinction and CCN concentrations are non-linearly related to size, complicating the retrieval of CCN based on extinction measurements (Ghan and Collins, 2004; Kapustin et al., 2006). It has been suggested from theory and an analysis of satellite retrievals (Nakajima et al., 2001) that

aerosol index (Deuze et al., 2001)

$$\mathrm{AI} = \mathrm{AOD} \times \alpha \quad (1)$$

where the Ångström parameter

$$\alpha = -\frac{\ln(\mathrm{AOD}_{\lambda_1}/\mathrm{AOD}_{\lambda_2})}{\ln(\lambda_1/\lambda_2)} \quad (2)$$

provides a superior proxy of CCN, as it gives lower weight to large (low α) aerosol and reduces the impact of large but low number-concentration sea salt and dust particles.

A significant body of prior work has evaluated the suitability of aerosol radiative properties as proxy for CCN based on local in-situ data and local remote sensing using sun-photometers or lidars. Feingold et al. (1998) developed a technique based on a combination of Doppler radar, microwave radiometer and lidar to infer CCN from the retrieved cloud droplet concentration, vertical velocity and lidar backscatter. Ghan and Collins (2004) devised a method for estimating CCN at cloud base from lidar retrievals and surface CCN measurements, which they evaluated in (Ghan et al., 2006) using aircraft, surface in-situ, and surface remote sensing measurements. The study highlighted deteriorating retrieval quality for higher supersaturations and for scenes with vertical inhomogeneity. A continental-scale compilation of co-located observations of AERONET sun-photometer (Holben et al., 1998) retrieved AOD and ground-based CCN measurements revealed a statistically robust power–law relationship between AOD and CCN for continental scales and (month) long averaging periods (Andreae, 2009). Limited-scale in-situ observations (Kapustin et al., 2006) showed that the relationship of AI to aerosol number and CCN is also strongly affected by relative humidity (increasing particle size and extinction but not aerosol number) and complex aerosol size distributions. An analysis of aircraft measurements for the ARCTAS measurement campaign over Canada showed reasonable temporal correlations between CCN and AOD ($r^2 = 0.59$) and a significant improvement in correlation when using in-situ dry extinction instead of vertically integrated ambient AOD (Shinozuka et al., 2015). An analysis of a large compilation of aircraft measurements over the Pacific revealed that regional campaign-average vertical profiles of extinction and CCN proxies show generally a strong correlation (Clarke and Kapustin, 2010) but it is unclear how representative this is for the temporal correlation of extinction and CCN at cloud base. Liu and Li (2014) investigated the correlation of CCN and aerosol radiative properties using data from five Atmospheric Radiation Measurement (ARM) Climate Research Facility sites. They found variable correlations between surface CCN and AERONET retrieved AOD for the different sites, with lower correlations for the Azores and Niger sites and attribute this to the dominance of large particles. They generally found improved correlations using AI as compared to AOD and best correlations between in-situ surface scattering/extinctions coefficients and in-situ measured scattering aerosol index. The importance of many of the above factors has also been realised in the context of deriving surface aerosol mass from AOD retrievals for air pollution applications over the continental United States (van Donkelaar et al., 2010), employing a chemical transport model to derive local linear conversion factors from AOD to surface mass.

In summary, previous work on the relationship between aerosol radiative properties and CCN has been based on in-situ CCN data in combination with aerosol radiative properties from in-situ measurements or remote sensing. Studies have found: a variable degree of correlations for different regions and aerosol regimes; generally improved correlations between AI and CCN as compared to AOD and CCN; a degradation of correlations in regions of high relative humidity; an impact of vertical layering on the correlation of surface CCN and aerosol radiative properties. However, the limited availability of direct measurements as well as their limited representativeness in the light of sampling errors (Schutgens et al., 2016b, a) has made it impossible to provide a global, statistically robust, assessment of the suitability of aerosol radiative properties as constraint for CCN. Consequently, no reliable global observational dataset of cloud condensation nuclei exists and a large body of literature uses AOD/AI almost synonymously for CCN.

This work provides a global assessment of the link between aerosol radiative properties and CCN, overcoming the insufficient global coverage of direct observations through use of a self-consistent global model (ECHAM-HAM, Stier et al., 2005, 2007; Zhang et al., 2012) of aerosol radiative properties and CCN. It is clear that no perfect global model of aerosol radiative properties or CCN exists (e.g. Myhre et al., 2013; Mann et al., 2014) so *self-consistent* in this context refers to the fact that the calculations of the aerosol radiative properties (based on Mie theory) and CCN (based on Köhler theory) are fully consistent in terms of the size-distribution, composition and mixing state, unaffected by any independent assumptions or errors common to remote sensing retrievals. Therefore, use of this model allows to consistently assess the relationship between aerosol radiative properties and CCN as biases in the simulated fields are expected to affect both parameters similarly. Nonetheless, it should be noted that the ability of models to mimic the spatial (in particular vertical) and temporal (co-)variability of aerosol and humidity fields introduces some quantitative uncertainty (Haywood et al., 1997).

While the introduced methodology would lend itself to the derivation of CCN retrieval from satellite retrieved aerosol radiative properties, this is not the focus of this study. Likewise, it should be pointed out that this work does not investigate the link between aerosol radiative properties and the number of activated cloud droplets, which additionally requires the knowledge of (highly uncertain) updraft velocities at cloud base or the point of activation. Instead, this work aims to provide the first consistent global analysis of the suit-

ability of aerosol radiative properties as observational constraint for CCN.

2 Methods

In this study we employ the aerosol-climate model ECHAM-HAM, version ECHAM-6.1_HAM-2.2, with a prognostic representation of the composition, size distribution, and mixing state of the major global aerosol components: sulfate, black carbon, particulate organic matter, sea salt, and mineral dust. More details and an extensive evaluation of this base model can be found in (Stier et al., 2005, 2007; Zhang et al., 2012; Schutgens and Stier, 2014) as well as part of the AeroCom intercomparison (Myhre et al., 2013; Stier et al., 2013; Mann et al., 2014).

2.1 The atmospheric general circulation model ECHAM6

The atmospheric general circulation model (GCM) ECHAM6 (Stevens et al., 2013) is the sixth-generation climate model developed at the Max Planck Institute for Meteorology. ECHAM6 solves prognostic equations for vorticity, divergence, surface pressure, and temperature, expressed in terms of spherical harmonics with a triangular truncation. Non linear processes and the physical parameterisations are solved on a corresponding Gaussian grid. Water vapour, cloud liquid water, cloud ice, and trace components are transported in grid-point space with a flux form semi-Lagrangian transport scheme (Lin and Rood, 1996). ECHAM6 contains a microphysical cloud scheme (Lohmann and Roeckner, 1996; Lohmann et al., 2007) with prognostic equations for cloud liquid water and ice. Cloud cover is represented using an assumed humidity distribution function (Sundqvist et al., 1989). Convective clouds and convective transport are based on the mass-flux scheme of Tiedtke (1989) with modifications by (Nordeng, 1994) and a modified triggering related to a prognostic treatment of the temperature variance in the planetary boundary layer (Stevens et al., 2013). Radiative transfer is represented using the rapid radiation transfer suite of models optimised for general circulation modeling (Iacono et al., 2008) with 16 and 14 bands in the longwave and shortwave parts of the spectrum, respectively.

2.2 The aerosol module HAM

The microphysical aerosol module HAM (Stier et al., 2005, 2007; Zhang et al., 2012) predicts the evolution of an ensemble of seven interacting internally- and externally-mixed log-normal aerosol modes. In the current setup, the components comprise: sulfate, black carbon, particulate organic matter, sea salt, and mineral dust. The microphysical core M7 (Vignati et al., 2004) calculates coagulation among the modes and the condensation of gas-phase sulfuric acid on the existing aerosol population. In the revised version HAM-2.0, the equilibrium water update is based on κ-Köhler theory (Petters and Kreidenweis, 2007) and a range of aerosol nucleation parameterisations have been introduced by Kazil et al. (2010) in addition to the original binary nucleation scheme. In this study we employ a parameterisation of neutral and charged nucleation Kazil and Lovejoy (2007) as described in Kazil et al. (2010). Aerosol radiative properties, as well as the sink processes of dry deposition, sedimentation, and wet deposition, are parameterised based on the prognostic aerosol size distribution, composition, and mixing state and coupled to the ECHAM meteorology. Emissions of mineral dust, sea salt and DMS from seawater are calculated online. For all other compounds, emission strength, distribution, and height are based on the AEROCOM aerosol model inter-comparison (http://aerocom.met.no) Phase II ACCMIP-MACCity emission inventory (Lamarque et al., 2010) for the year 2000. We implement an explicit Köhler theory based activation scheme with empirical estimation of maximum supersaturation in updrafts derived from explicit parcel model calculations (Abdul-Razzak and Ghan, 2000). The total number of activated particles is calculated as sum of the integrated log-normal aerosol number distribution from the radius of activation for each mode. Köhler theory requires detailed information about the aerosol composition. While the composition is relatively well defined for some aerosol components, such as sea salt, the detailed composition of other components, such as particulate organic matter is insufficiently understood. In many measurements of aerosol chemical composition, a non-negligible fraction of the aerosol mass cannot be identified and is often attributed to organics (Jimenez et al., 2009). Given the large uncertainties in the identification and simulation of organics, as well as low measured κ values (Petters and Kreidenweis, 2007), we ignore ionic contributions of organics to the solute and treat organics as well as dust in the hydrophilic modes as wettable and in the hydrophobic modes as entirely hydrophobic.

2.2.1 Cloud Condensation Nuclei

In addition to the application of Köhler theory in the activation scheme of HAM, this scheme is also used for a consistent diagnostics of cloud condensation nuclei at fixed, prescribed supersaturations.

2.2.2 Aerosol radiative properties

Aerosol radiative properties are calculated in the framework of Mie theory. For each aerosol mode, effective refractive indices are calculated by volume-averaging the refractive indices of all components, including aerosol water, which is parameterised in terms of ambient relative humidity. The effective complex refractive indices and the Mie size-parameters for each mode serve as input to look-up tables for the aerosol radiative properties, providing extinc-

tion cross-section, single scattering albedo, and asymmetry parameter to the ECHAM radiation scheme. Long-wave (LW) radiative properties have been introduced and coupled to the ECHAM LW radiation scheme and black carbon refractive indices have been revised for version HAM-2.0 (Stier et al., 2007). We additionally introduce diagnostics of: Aerosol Index (AI) calculated online from the aerosol optical depth at wavelengths comparable to the MODIS AI product: AI = AOD $\times\alpha$, where the Ångström parameter $\alpha = -\frac{\ln(\mathrm{AOD}_{550\mathrm{nm}}/\mathrm{AOD}_{865\mathrm{nm}})}{\ln(\lambda_{550\mathrm{nm}}/\lambda_{865\mathrm{nm}})}$; fine mode AOD calculated as sum of Aitken and Accumulation mode AOD; dry AOD approximated from total AOD minus the AOD times the volume fraction of aerosol water.

We further investigate the role of the vertical aerosol distribution using the local (model layer) aerosol extinction coefficient (AEC) as well as the extinction aerosol index ($\mathrm{AI}_{\mathrm{AEC}}$), defined here as local aerosol extinction coefficient times the local Ångström parameter: $\mathrm{AI}_{\mathrm{AEC}}$=AEC$\times\alpha_{AEC}$, where $\alpha_{AEC} = -\frac{\ln(\mathrm{AEC}_{550\mathrm{nm}}/\mathrm{AEC}_{865\mathrm{nm}})}{\ln(\lambda_{550\mathrm{nm}}/\lambda_{865\mathrm{nm}})}$ is evaluated from the local aerosol extinction coefficients, instead of from the column integrated aerosol optical depths used in AI.

2.3 Simulation setup

All simulations were performed from October 1999 to December 2000 and constrain the large-scale meteorology to the year 2000 by nudging (Jeuken et al., 1996) the model to the ECMWF ERA40 reanalysis data (Simmons and Gibson, 2000). Only the year 2000 data are analysed. We employ a horizontal resolution of T63 in spectral space with a corresponding resolution of $1.8^\circ \times 1.8^\circ$ on a Gaussian grid. The vertical resolution is set to 31 levels, extending from the surface up to 10 hPa.

2.4 Statistical analysis

The statistical analysis is performed on 6 hourly instantaneous model output, unless longer averaging periods are described. Correlations are reported as linear Pearson correlation coefficient of log-transformed parameters, providing consistency with the majority of prior work. Fits are derived from linear regression of the log-transformed parameters to derive power-law expressions. Note that the results remain largely unchanged when using the non-parametric Spearman's rank correlation coefficient (Fig. 7e).

3 Results

The ECHAM-HAM simulated annual-mean surface CCN concentrations (Fig. 1) show distinct land–sea contrast, with maxima over the main aerosol source areas. CCN concentrations at the lower 0.2 % supersaturation (activating only the larger particles of the CCN spectrum into cloud droplets) are lower than at the higher supersaturation of 1.5 % (also activating smaller particles of the CCN spectrum).

The corresponding annual-mean AOD (Fig. 2a) shows similar maxima in the main aerosol source areas. However, it also shows high values over the sea-salt aerosol dominated storm track regions, dust source regions, such as the Saharan dust outflow, and generally higher levels downwind of the source areas (mainly because AOD is a column integrated quantity while (Fig. 1) shows surface CCN values). AI, giving lower weight to large particles, is in better spatial agreement with the annual mean CCN distribution than AOD (Fig. 2b).

These results confirm the common understanding that CCN are related to AOD and (better) to AI for large spatial scales and long averaging periods. This is also confirmed in the fit of regional annual mean AOD and CCN pairs (Fig. 4a) for the main continents defined in Fig. 3.

The derived fit of the mean values ($y = 0.0002x^{1.074}$ for $\mathrm{CCN}_{0.5\%}$) is statistically robust ($r^2 = 0.70$) and compares to a fit of campaign mean co-located surface based CCN measurements and AERONET sun-photometer retrievals of AOD ($y = 0.0027x^{0.640}$ for $\mathrm{CCN}_{0.4\%}$, $r^2 = 0.88$, Andreae, 2009). The inclusion of oceanic regions dominated by large sea salt particles with high extinction per particle, deteriorates the relationship of AOD and $\mathrm{CCN}_{0.2\%}$ (Fig. 4b) and r^2 decreases from 0.65 to 0.47. The fit for land and ocean regions combined (Fig. 4c) improves using AI instead of AOD ($r^2 = 0.84$).

Despite the good fit of the regional annual mean CCN and AI, the fit of individual monthly means within each region (colour coded scatter and fits in Fig. 4a) is variable, with r ranging from 0.41 to 0.93 for individual regions.

The mean goodness of fit deteriorates from $r^2 = 0.57$ to $r^2 = 0.46$ and $r^2 = 0.41$ when varying the averaging periods of CCN and AI pairs from monthly via daily to 6 h instantaneous data (Fig. 5).

The global distribution of (temporal) Pearson's correlation coefficients between surface $\mathrm{CCN}_{0.2\%}$ and vertically integrated aerosol optical depth (map in Fig. 6) reveals variable suitability of vertically integrated AOD as proxy for surface CCN. While correlations are generally positive and exceed $r = 0.6$ for large parts of the high latitudes and the tropical oceans, significant areas of the continents and subtropical subsidence regions show low or even negative correlations.

A number of alternative aerosol radiative properties have been proposed to provide superior proxies of CCN. Note that maps of their correlations and the corresponding global mean values (Fig. 7), specifically of (b) fine mode aerosol optical depth ($\overline{r} = 0.50$), (c) dry aerosol optical depth ($\overline{r} = 0.45$) and (d) aerosol index ($\overline{r} = 0.53$) do not show significantly improved correlations as compared to (a) aerosol optical depth ($\overline{r} = 0.44$). Usage of the non-parametric Spearman's rank correlation coefficient (e) gives very similar correlations ($\overline{\rho} = 0.41$). Sampling $\mathrm{CCN}_{0.2\%}$ at the model simulated lowest cloud base gives slightly reduced ($\overline{r} = 0.36$) but spatially very similar correlations with AOD (f).

The analysis of the vertical structure of aerosol extinction and CCN reveals the reasons for the large spatial variability in these correlations (Fig. 6). In agreement with observations (Clarke and Kapustin, 2010), the correlation between the annual mean vertical profiles of the aerosol extinction coefficient (AEC) and CCN is robust (r ranges from 0.84 to 0.98 for the selected regions), even in areas for which the temporal correlation of column integrated AOD and surface CCN is poor, such as the South-East Atlantic. This can be explained by vertical decoupling: while the temporal correlation of surface CCN with vertically integrated AOD is low ($r \approx 0.2$) in this region, the correlation of surface CCN with the surface extinction coefficient is robust ($r > 0.6$). Generally, the temporal correlation of extinction coefficients with CCN at the same layer (orange) is significantly stronger than the correlation of CCN at each layer with vertically integrated AOD (red). The extinction coefficient is temporally well correlated with relative humidity throughout the troposphere (pink). The correlation of vertically integrated AOD with CCN at cloud base is generally comparable to the correlation with surface CCN. For the Indian region, surface level CCN are even anti-correlated with vertically integrated AOD. Here, surface level extinction is strongly correlated with relative humidity (pink), while surface level CCN are efficiently removed by scavenging during high relative humidity events associated with strong precipitation. Over Europe and North America, correlations of column integrated AOD and surface CCN are generally intermediate to high, in particular north of the sub-tropical subsidence areas. Correlations of extinction coefficients with relative humidity are higher over Europe than over North American and particularly higher than over South America, where the predominant carbonaceous aerosols take up relatively little water. Interestingly, correlations of extinction coefficients with relative humidity are also low for the Southern Ocean region, despite the fact that the dominant (by extinction) sea salt aerosol is highly hygroscopic. This is likely due to the fact that not only aerosol water uptake but also aerosol removal via scavenging is positively correlated to relative humidity (via clouds and precipitation). This hypothesis is supported by the drop off of this correlation around and below cloud base (green line). However, correlations of column integrated AOD and surface CCN are consistently high for this region as well as for the northern high-latitude oceans.

These results suggest that vertically integrated aerosol radiative properties, as retrieved from satellite imagers, are of limited suitability as proxy for global surface or cloud base CCN: 71 % of the area of the globe shows correlation coefficients between $\mathrm{CCN}_{0.2\%}$ at cloud base and AOD below 0.5 (i.e. AOD variability explains only 25 % of the CCN variance). The fractional area of $r < 0.5$ increases to 83 and 96 % for $\mathrm{CCN}_{0.5\%}$ and $\mathrm{CCN}_{1.5\%}$, respectively. Corresponding areas for $r < 0.5$ between CCN and aerosol index are somewhat lower (52, 66, 91 % for $\mathrm{CCN}_{0.2\%}$, $\mathrm{CCN}_{0.5\%}$, $\mathrm{CCN}_{1.5\%}$, respectively, Fig. 8).

Could vertically resolved aerosol radiative properties, e.g. from space-born lidars, provide stronger constraints on CCN and ultimately the radiative effect of aerosol cloud interactions?

The correlation of surface CCN with surface aerosol extinction coefficients (AEC) (Fig. 9a) is significantly improved for most of the globe. This highlights the important role of the aerosol vertical distribution for determining CCN at specific altitudes. Correlations further improve for surface extinction aerosol index $\mathrm{AI}_{\mathrm{AEC}}$ (Fig. 9b) with $r > 0.8$ for most of the globe. This can be attributed to the lower weight AI gives to large aerosols, reducing the impact of low number-concentration sea salt and dust particles.

Note that correlations between surface layer CCN and $\mathrm{AI}_{\mathrm{AEC}}$ also deteriorate for higher supersaturations (sampling the smaller Aitken mode range of the aerosol size distribution), as expected from Mie theory, as the smaller particles selected by higher supersaturations contribute less to total extinction (Fig. 10). This is particularly evident over the continents with significant primary fine mode aerosol emissions.

4 Conclusions

Direct measurements of cloud condensation nuclei are limited and sample only a very small fraction of the globe so that remote sensing from satellites and ground based instruments is widely used as a proxy for cloud condensation nuclei. However, the underlying assumptions cannot be robustly tested with the small number of measurements available so that no reliable global estimate of cloud condensation nuclei exists.

This study overcomes this limitation using a self-consistent global model (ECHAM-HAM) of aerosol radiative properties and cloud condensation nuclei.

An analysis of the correlation of simulated aerosol radiative properties and cloud condensation nuclei confirms findings from earlier work that continental mean CCN are related to AOD ($r^2 = 0.65$) for large (continental) spatial scales and long (monthly) averaging periods but r^2 drops to 0.47 when oceanic regions are included. Use of AI improves the goodness of fit, including oceanic regions, to $r^2 = 0.84$.

The mean goodness of fit for CCN and AI pairs over continental and oceanic regions deteriorates from $r^2 = 0.57$ to $r^2 = 0.46$ and $r^2 = 0.41$ varying the averaging period from monthly via daily to 6 h instantaneous data.

However, aerosol–cloud interactions occur locally (e.g. McComiskey and Feingold, 2012): according to this analysis, the temporal correlation on the local (global-model grid) scale 71 % of the area of the globe shows correlation coefficients between $\mathrm{CCN}_{0.2\%}$ at cloud base and AOD below 0.5 (i.e. AOD variability explains only 25 % of the CCN variance). The areas with low correlations include the main marine stratocumulus decks, considered most susceptible to aerosol perturbations (Boucher et al., 2013). This suggests

that constraints from passive satellite remote sensing are particularly limited in areas key for radiative forcing due to aerosol–cloud interactions. Note that correlations for alternative aerosol radiative properties proposed as superior proxies of CCN such as fine mode aerosol optical depth, dry aerosol optical depth and aerosol index do not show significant improvements.

A number of reasons contribute to the low correlations between aerosol radiative properties and CCN, in particular over sub-tropical subsidence areas: aerosol extinction is heavily affected by humidity, in particular at cloud base, and often the local correlation of relative humidity with aerosol extinction coefficients is larger than the correlation of local CCN with column integrated AOD. Satellite retrievals based on visible wavelengths are most sensitive to larger particles, corresponding to CCN at small supersaturations. Correlations between CCN and AI decrease with increasing supersaturations, in particular over the continents with significant primary fine mode aerosol emissions. Additionally, surface or cloud-base CCN and column AOD are often decoupled: and correlations of CCN with local aerosol extinction coefficients throughout the troposphere significantly exceed the correlations with column AOD. Consequently, correlations of surface CCN with surface AEC are significantly larger than with column AOD and are further improved for surface $\mathrm{AI}_{\mathrm{AEC}}$ for which $r > 0.8$ for most of the globe.

While the ability of this global model to mimic the spatial (in particular vertical) and temporal (co-)variability of aerosol and humidity fields introduces quantitative uncertainty, it should be noted that this self-consistent approach is free from retrieval errors, which would add additional uncertainty when using real satellite data. Advances in computational capabilities now make high-resolution, large-domain simulations of aerosols, clouds and their interactions possible. Such simulations should be increasingly used to test common assumptions in the assessment of aerosol cloud interactions from space (e.g. Gryspeerdt et al., 2015).

The findings in this work have important implications for satellite based studies of aerosol–cloud interactions. They suggest that vertically resolved remote sensing techniques, such as satellite-based high-spectral resolution lidars as ATLID on the ESA/JAXA EarthCare satellite, have a large potential for global monitoring of cloud condensation nuclei. The additional improvement in correlations using the dual-wavelength extinction measurements in AI, suggests that multi-wavelength high-spectral resolution lidars, such as the NASA airborne HSRL (McPherson et al., 2010), could further advance observational constraints on CCN from space.

While the sparse sampling of lidars from space (the CALIOP space-born lidar, Winker et al., 2009, samples the globe sparsely in 16 days, in comparison to e-folding aerosol lifetimes ranging from about $1/2$ day for sea salt to 7 days for black carbon, Textor et al., 2006) may introduce sampling errors, these could be potentially mitigated through synergistic retrievals with co-located imaging radiometers. Ultimately, the assimilation into global aerosol models may provide the best observationally constrained dataset of global cloud condensation nuclei.

Acknowledgements. I would like to thank Johannes Quaas (University of Leipzig), Nick Schutgens and Zak Kipling (both University of Oxford) for comments on the manuscript and Yohei Shinozuka (NASA Ames) for helpful discussions. The research leading to these results has received funding from the European Research Council under the European Union's Seventh Framework Programme (FP7/2007–2013)/ERC grant agreement no. FP7- 280025. The simulations were performed using the ARCHER UK National Supercomputing Service.

References

Abdul-Razzak, H. and Ghan, S. J.: A parameterization of aerosol activation 2. Multiple aerosol types, J. Geophys. Res., 105, 6837–6844, 2000.

Albrecht, B. A.: Aerosols, cloud microphysics, and fractional cloudiness, Science, 245, 1227–1230, 1989.

Andreae, M. O.: Correlation between cloud condensation nuclei concentration and aerosol optical thickness in remote and polluted regions, Atmos. Chem. Phys., 9, 543–556, doi:10.5194/acp-9-543-2009, 2009.

Boucher, O., Randall, D., Artaxo, P., Bretherton, C., Feingold, G., Forster, P., Kerminen, V.-M., Kondo, Y., Liao, H., Lohmann, U., Rasch, P., Satheesh, S., Sherwood, S., Stevens, B., Zhang, X., Bala, G., Bellouin, N., Benedetti, A., Bony, S., Caldeira, K., Genio, A. D., Facchini, M., Flanner, M., Ghan, S., Granier, C., Hoose, C., Jones, A., Koike, M., Kravitz, B., Laken, B., Lebsock, M., Mahowald, N., Myhre, G., Robock, C. O. A., Samset, B., Schmidt, H., Schulz, M., Stephens, G., Stier, P., Storelvmo, T., Winker, D., and Wyant, M.: Clouds and Aerosols, in: Climate Change 2013: The Physical Science Basis. Contribution of Working Group I to the Fifth Assessment Report of the Intergovernmental Panel on Climate Change, Cambridge University Press, Cambridge, UK and New York, NY, USA, 2013.

Clarke, A. and Kapustin, V.: Hemispheric aerosol vertical profiles: anthropogenic impacts on optical depth and cloud nuclei, Science, 330, 1047–1047, 2010.

Deuze, J. L., Breon, F. M., Devaux, C., Goloub, P., Herman, M., Lafrance, B., Maignan, F., Marchand, A., Nadal, F., Perry, G., and Tanre, D.: Remote sensing of aerosols over land surfaces from POLDER-ADEOS-1 polarized measurements, J. Geophys. Res.-Atmos., 106, 4913–4926, doi:10.1029/2000jd900364, 2001.

Feingold, G., Yang, S., Hardesty, R. M., and Cotton, W. R.: Feasibility of Retrieving Cloud Condensation Nucleus Properties from Doppler Cloud Radar, Microwave Radiometer, and Lidar, Journal of Atmospheric and Oceanic Technology, 15, 1188–1195, doi:10.1175/1520-0426(1998)015<1188:FORCCN>2.0.CO;2, 1998.

Ghan, S. J. and Collins, D. R.: Use of in situ data to test a Raman lidar-based cloud condensation nuclei remote sensing method, J. Atmos. Ocean. Tech., 21, 387–394, 2004.

Ghan, S. J., Rissman, T. A., Elleman, R., Ferrare, R. A., Turner, D., Flynn, C., Wang, J., Ogren, J., Hudson, J., Jonsson, H. H., Van-

Reken, T., Flagan, R. C., and Seinfeld, J. H.: Use of in situ cloud condensation nuclei, extinction, and aerosol size distribution measurements to test a method for retrieving cloud condensation nuclei profiles from surface measurements, J. Geophys. Res.-Atmos., 111, D05S10, doi:10.1029/2004JD005752, 2006.

Grandey, B. S. and Stier, P.: A critical look at spatial scale choices in satellite-based aerosol indirect effect studies, Atmos. Chem. Phys. Discuss., 10, 15417–15440, doi:10.5194/acpd-10-15417-2010, 2010.

Gryspeerdt, E., Stier, P., and Grandey, B. S.: Cloud fraction mediates the aerosol optical depth-cloud top height relationship, Geophys. Res. Lett., 41, 3622–3627, doi:10.1002/2014gl059524, 2014.

Gryspeerdt, E., Stier, P., White, B. A., and Kipling, Z.: Wet scavenging limits the detection of aerosol effects on precipitation, Atmos. Chem. Phys., 15, 7557–7570, doi:10.5194/acp-15-7557-2015, 2015.

Haywood, J. M., Roberts, D. L., Slingo, A., Edwards, J. M., and Shine, K. P.: General circulation model calculations of the direct radiative forcing by anthropogenic sulfate and fossil-fuel soot aerosol, J. Clim., 10, 1562–1577, 1997.

Holben, B., Eck, T., Slutsker, I., Tanre, D., Buis, J., Setzer, A., Vermote, E., Reagan, J., Kaufman, Y., Nakajima, T., Lavenu, F., Jankowiak, I., and Smirnov, A.: AERONET – A federated instrument network and data archive for aerosol characterization, Remote Sens. Environ., 66, 1–16, 1998.

Iacono, M., Delamere, J. S., Mlawer, E. J., Shephard, M. W., Clough, S. A., and Collins, W. D.: Radiative forcing by long-lived greenhouse gases: calculations with the AER radiative transfer models, J. Geophys. Res., 113, D13103, doi:10.1029/2008jd009944, 2008.

Jeuken, A. B. M., Siegmund, P. C., Heijboer, L. C., Feichter, J., and Bengtsson, L.: On the potential of assimilating meteorological analyses in a global climate model for the purpose of model validation, J. Geophys. Res., 101, 16939–16950, doi:10.1029/96JD01218, 1996.

Jimenez, J. L., Canagaratna, M. R., Donahue, N. M., Prevot, A. S. H., Zhang, Q., Kroll, J. H., DeCarlo, P. F., Allan, J. D., Coe, H., Ng, N. L., Aiken, A. C., Docherty, K. S., Ulbrich, I. M., Grieshop, A. P., Robinson, A. L., Duplissy, J., Smith, J. D., Wilson, K. R., Lanz, V. A., Hueglin, C., Sun, Y. L., Tian, J., Laaksonen, A., Raatikainen, T., Rautiainen, J., Vaattovaara, P., Ehn, M., Kulmala, M., Tomlinson, J. M., Collins, D. R., Cubison, M. J., E., Dunlea, J., Huffman, J. A., Onasch, T. B., Alfarra, M. R., Williams, P. I., Bower, K., Kondo, Y., Schneider, J., Drewnick, F., Borrmann, S., Weimer, S., Demerjian, K., Salcedo, D., Cottrell, L., Griffin, R., Takami, A., Miyoshi, T., Hatakeyama, S., Shimono, A., Sun, J. Y., Zhang, Y. M., Dzepina, K., Kimmel, J. R., Sueper, D., Jayne, J. T., Herndon, S. C., Trimborn, A. M., Williams, L. R., Wood, E. C., Middlebrook, A. M., Kolb, C. E., Baltensperger, U., and Worsnop, D. R.: Evolution of Organic Aerosols in the Atmosphere, Science, 326, 1525–1529, doi:10.1126/science.1180353, 2009.

Kapustin, V. N., Clarke, A. D., Shinozuka, Y., Howell, S., Brekhovskikh, V., Nakajima, T., and Higurashi, A.: On the determination of a cloud condensation nuclei from satellite: Challenges and possibilities, J. Geophys. Res.-Atmos., 111, D04202, doi:10.1029/2004jd005527, 2006.

Kaufman, Y. J. and Nakajima, T.: Effect of amazon smoke on cloud microphysics and albedo – Analysis from satellite imagery, J. Appl. Meteorol., 32, 729–744, 1993.

Kaufman, Y. J., Boucher, O., Tanré, D., Chin, M., Remer, L. A., and Takemura, T.: Aerosol anthropogenic component estimated from satellite data, Geophys. Res. Lett., 32, L17804, doi:10.1029/2005GL023125, 2005.

Kazil, J. and Lovejoy, E. R.: A semi-analytical method for calculating rates of new sulfate aerosol formation from the gas phase, Atmos. Chem. Phys., 7, 3447–3459, doi:10.5194/acp-7-3447-2007, 2007.

Kazil, J., Stier, P., Zhang, K., Quaas, J., Kinne, S., O'Donnell, D., Rast, S., Esch, M., Ferrachat, S., Lohmann, U., and Feichter, J.: Aerosol nucleation and its role for clouds and Earth's radiative forcing in the aerosol-climate model ECHAM5-HAM, Atmos. Chem. Phys., 10, 10733–10752, doi:10.5194/acp-10-10733-2010, 2010.

Lamarque, J.-F., Bond, T. C., Eyring, V., Granier, C., Heil, A., Klimont, Z., Lee, D., Liousse, C., Mieville, A., Owen, B., Schultz, M. G., Shindell, D., Smith, S. J., Stehfest, E., Van Aardenne, J., Cooper, O. R., Kainuma, M., Mahowald, N., McConnell, J. R., Naik, V., Riahi, K., and van Vuuren, D. P.: Historical (1850–2000) gridded anthropogenic and biomass burning emissions of reactive gases and aerosols: methodology and application, Atmos. Chem. Phys., 10, 7017–7039, doi:10.5194/acp-10-7017-2010, 2010.

Lin, S. J. and Rood, R. B.: Multidimensional flux form semi-Lagrangian transport, Mon. Weather Rev., 124, 2046–2068, 1996.

Liu, Jianjun and Li, Zhanqing: Estimation of cloud condensation nuclei concentration from aerosol optical quantities: influential factors and uncertainties, Atmos. Chem. Phys., 14, 471–483, doi:10.5194/acp-14-471-2014, 2014.

Lohmann, U. and Feichter, J.: Global indirect aerosol effects: a review, Atmos. Chem. Phys., 5, 715–737, doi:10.5194/acp-5-715-2005, 2005.

Lohmann, U. and Roeckner, E.: Design and performance of a new cloud microphysics scheme developed for the ECHAM4 general circulation model, Clim. Dynam., 12, 557–572, 1996.

Lohmann, U., Stier, P., Hoose, C., Ferrachat, S., Kloster, S., Roeckner, E., and Zhang, J.: Cloud microphysics and aerosol indirect effects in the global climate model ECHAM5-HAM, Atmos. Chem. Phys., 7, 3425–3446, doi:10.5194/acp-7-3425-2007, 2007.

Mann, G. W., Carslaw, K. S., Reddington, C. L., Pringle, K. J., Schulz, M., Asmi, A., Spracklen, D. V., Ridley, D. A., Woodhouse, M. T., Lee, L. A., Zhang, K., Ghan, S. J., Easter, R. C., Liu, X., Stier, P., Lee, Y. H., Adams, P. J., Tost, H., Lelieveld, J., Bauer, S. E., Tsigaridis, K., van Noije, T. P. C., Strunk, A., Vignati, E., Bellouin, N., Dalvi, M., Johnson, C. E., Bergman, T., Kokkola, H., von Salzen, K., Yu, F., Luo, G., Petzold, A., Heintzenberg, J., Clarke, A., Ogren, J. A., Gras, J., Baltensperger, U., Kaminski, U., Jennings, S. G., O'Dowd, C. D., Harrison, R. M., Beddows, D. C. S., Kulmala, M., Viisanen, Y., Ulevicius, V., Mihalopoulos, N., Zdimal, V., Fiebig, M., Hansson, H.-C., Swietlicki, E., and Henzing, J. S.: Intercomparison and evaluation of global aerosol microphysical properties among AeroCom models of a range of complexity, Atmos. Chem. Phys., 14, 4679–4713, doi:10.5194/acp-14-4679-2014, 2014.

McComiskey, A. and Feingold, G.: The scale problem in quantifying aerosol indirect effects, Atmos. Chem. Phys., 12, 1031–1049, doi:10.5194/acp-12-1031-2012, 2012.

McPherson, C., Reagan, J., Hostetler, C., Hair, J., and Ferrare, R.: Progress in the validation of dual-wavelength aerosol retrieval models via airborne high spectral resolution lidar data, in: 2010 IEEE International Geoscience and Remote Sensing Symposium, IEEE International Symposium on Geoscience and Remote Sensing IGARSS, 1714–1717, doi:10.1109/IGARSS.2010.5648851, Honolulu, HI, 25–30 June, 2010.

Myhre, G., Samset, B. H., Schulz, M., Balkanski, Y., Bauer, S., Berntsen, T. K., Bian, H., Bellouin, N., Chin, M., Diehl, T., Easter, R. C., Feichter, J., Ghan, S. J., Hauglustaine, D., Iversen, T., Kinne, S., Kirkevåg, A., Lamarque, J.-F., Lin, G., Liu, X., Lund, M. T., Luo, G., Ma, X., van Noije, T., Penner, J. E., Rasch, P. J., Ruiz, A., Seland, Ø., Skeie, R. B., Stier, P., Takemura, T., Tsigaridis, K., Wang, P., Wang, Z., Xu, L., Yu, H., Yu, F., Yoon, J.-H., Zhang, K., Zhang, H., and Zhou, C.: Radiative forcing of the direct aerosol effect from AeroCom Phase II simulations, Atmos. Chem. Phys., 13, 1853–1877, doi:10.5194/acp-13-1853-2013, 2013.

Nakajima, T., Higurashi, A., Kawamoto, K., and Penner, J. E.: A possible correlation between satellite-derived cloud and aerosol microphysical parameters, Geophys. Res. Lett., 28, 1171–1174, doi:10.1029/2000gl012186, 2001.

Nordeng, T. E.: Extended versions of the convective parameterization scheme at ECMWF and their impact on the mean and transient activity of the model in the tropics, Technical Memorandum 206, ECMWF, Reading, UK, 42 pp., 1994.

Petters, M. D. and Kreidenweis, S. M.: A single parameter representation of hygroscopic growth and cloud condensation nucleus activity, Atmos. Chem. Phys., 7, 1961–1971, doi:10.5194/acp-7-1961-2007, 2007.

Rosenfeld, D., Lohmann, U., Raga, G. B., O'Dowd, C. D., Kulmala, M., Fuzzi, S., Reissell, A., and Andreae, M. O.: Flood or drought: how do aerosols affect precipitation?, Science, 321, 1309–1313, 2008.

Schutgens, N. A. J. and Stier, P.: A pathway analysis of global aerosol processes, Atmos. Chem. Phys., 14, 11657–11686, doi:10.5194/acp-14-11657-2014, 2014.

Schutgens, N. A. J., Gryspeerdt, E., Weigum, N., Tsyro, S., Goto, D., Schulz, M., and Stier, P.: Will a perfect model agree with perfect observations? The impact of spatial sampling, Atmospheric Chemistry and Physics Discussions, 2016, 1–32, doi:10.5194/acp-2015-973, http://www.atmos-chem-phys-discuss.net/acp-2015-973/, 2016a.

Schutgens, N. A. J., Partridge, D. G., and Stier, P.: The importance of temporal collocation for the evaluation of aerosol models with observations, Atmospheric Chemistry and Physics, 16, 1065–1079, doi:10.5194/acp-16-1065-2016, http://www.atmos-chem-phys.net/16/1065/2016/, 2016b.

Shinozuka, Y., Clarke, A. D., Nenes, A., Jefferson, A., Wood, R., McNaughton, C. S., Ström, J., Tunved, P., Redemann, J., Thornhill, K. L., Moore, R. H., Lathem, T. L., Lin, J. J., and Yoon, Y. J.: The relationship between cloud condensation nuclei (CCN) concentration and light extinction of dried particles: indications of underlying aerosol processes and implications for satellite-based CCN estimates, Atmos. Chem. Phys., 15, 7585–7604, doi:10.5194/acp-15-7585-2015, 2015.

Simmons, A. J. and Gibson, J. K.: The ERA-40 project plan, ERA-40 Project Report Series 1, ECMWF, Shinfield Park, Reading, UK, 2000.

Spracklen, D. V., Carslaw, K. S., Pöschl, U., Rap, A., and Forster, P. M.: Global cloud condensation nuclei influenced by carbonaceous combustion aerosol, Atmos. Chem. Phys., 11, 9067–9087, doi:10.5194/acp-11-9067-2011, 2011.

Stevens, B. and Feingold, G.: Untangling aerosol effects on clouds and precipitation in a buffered system, Nature, 461, 607–613, doi:10.1038/Nature08281, 2009.

Stevens, B., Giorgetta, M., Esch, M., Mauritsen, T., Crueger, T., Salzmann, S. R. M., Schmidt, H., Bader, J., Block, K., Brokopf, R., Fast, I., Kinne, S., Kornblueh, L., Lohmann, U., Pincus, R., Reichler, T., and Roeckner, E.: Atmospheric component of the MPI-M Earth System Model: ECHAM6, J. Adv. Model. Earth Syst., 5, 146–172, doi:10.1002/jame.20015, 2013.

Stier, P., Feichter, J., Kinne, S., Kloster, S., Vignati, E., Wilson, J., Ganzeveld, L., Tegen, I., Werner, M., Balkanski, Y., Schulz, M., Boucher, O., Minikin, A., and Petzold, A.: The aerosol-climate model ECHAM5-HAM, Atmos. Chem. Phys., 5, 1125–1156, doi:10.5194/acp-5-1125-2005, 2005.

Stier, P., Seinfeld, J. H., Kinne, S., and Boucher, O.: Aerosol absorption and radiative forcing, Atmos. Chem. Phys., 7, 5237–5261, doi:10.5194/acp-7-5237-2007, 2007.

Stier, P., Schutgens, N. A. J., Bellouin, N., Bian, H., Boucher, O., Chin, M., Ghan, S., Huneeus, N., Kinne, S., Lin, G., Ma, X., Myhre, G., Penner, J. E., Randles, C. A., Samset, B., Schulz, M., Takemura, T., Yu, F., Yu, H., and Zhou, C.: Host model uncertainties in aerosol radiative forcing estimates: results from the AeroCom Prescribed intercomparison study, Atmos. Chem. Phys., 13, 3245–3270, doi:10.5194/acp-13-3245-2013, 2013.

Sundqvist, H., Berge, E., and Kristjansson, J.: Condensation and cloud parameterization studies with a mesoscale numerical weather prediction model, Mon. Weather Rev., 117, 1641–1657, 1989.

Textor, C., Schulz, M., Guibert, S., Kinne, S., Balkanski, Y., Bauer, S., Berntsen, T., Berglen, T., Boucher, O., Chin, M., Dentener, F., Diehl, T., Easter, R., Feichter, H., Fillmore, D., Ghan, S., Ginoux, P., Gong, S., Grini, A., Hendricks, J., Horowitz, L., Huang, P., Isaksen, I., Iversen, I., Kloster, S., Koch, D., Kirkevåg, A., Kristjansson, J. E., Krol, M., Lauer, A., Lamarque, J. F., Liu, X., Montanaro, V., Myhre, G., Penner, J., Pitari, G., Reddy, S., Seland, Ø., Stier, P., Takemura, T., and Tie, X.: Analysis and quantification of the diversities of aerosol life cycles within AeroCom, Atmos. Chem. Phys., 6, 1777–1813, doi:10.5194/acp-6-1777-2006, 2006.

Tiedtke, M.: A comprehensive mass flux scheme for cumulus parameterization in large scale models, Mon. Weather Rev., 117, 1779–1800, 1989.

Twomey, S.: Pollution and the planetary albedo, Atmos. Environ., 8, 1251–1256, 1974.

van Donkelaar, A., Martin, R. V., Brauer, M., Kahn, R., Levy, R., Verduzco, C., and Villeneuve, P. J.: Global estimates of ambient fine particulate matter concentrations from satellite-based aerosol optical depth: development and application, Environ. Health Persp., 118, 847–855, doi:10.1289/ehp.0901623, 2010.

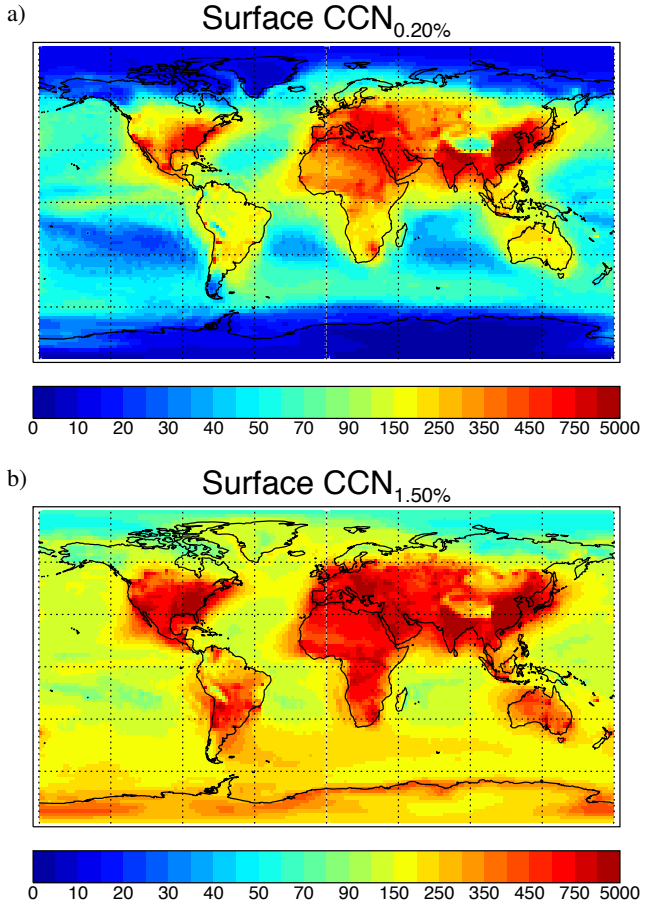

Figure 1. Annual-mean ECHAM-HAM simulated surface cloud condensation nuclei concentrations [cm^{-3}] at **(a)** 0.2 % and **(b)** 1.5 % supersaturation.

Vignati, E., Wilson, J., and Stier, P.: M7: a size resolved aerosol mixture module for the use in global aerosol models, J. Geophys. Res., 109, D22202, doi:10.1029/2003JD004485, 2004.

Winker, D. M., Vaughan, M. A., Omar, A., Hu, Y. X., Powell, K. A., Liu, Z. Y., Hunt, W. H., and Young, S. A.: Overview of the CALIPSO Mission and CALIOP Data Processing Algorithms, J. Atmos. Ocean. Tech., 26, 2310–2323, doi:10.1175/2009jtecha1281.1, 2009.

Zhang, K., O'Donnell, D., Kazil, J., Stier, P., Kinne, S., Lohmann, U., Ferrachat, S., Croft, B., Quaas, J., Wan, H., Rast, S., and Feichter, J.: The global aerosol-climate model ECHAM-HAM, version 2: sensitivity to improvements in process representations, Atmos. Chem. Phys., 12, 8911–8949, doi:10.5194/acp-12-8911-2012, 2012.

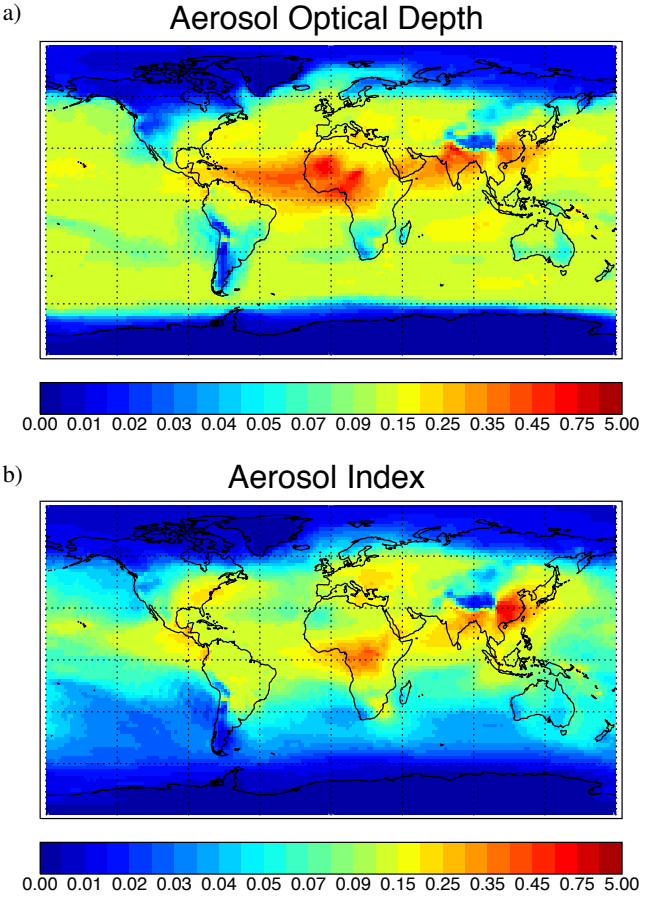

Figure 2. Annual-mean ECHAM-HAM simulated **(a)** aerosol optical depth at 550nm and **(b)** aerosol index between wavelengths of 550 and 865nm. Note the non-linear scale, comparable to Fig. 1.

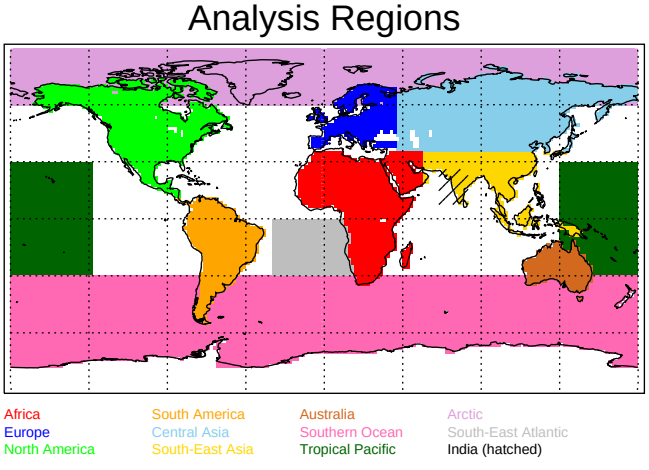

Figure 3. Map of regions used in the analysis.

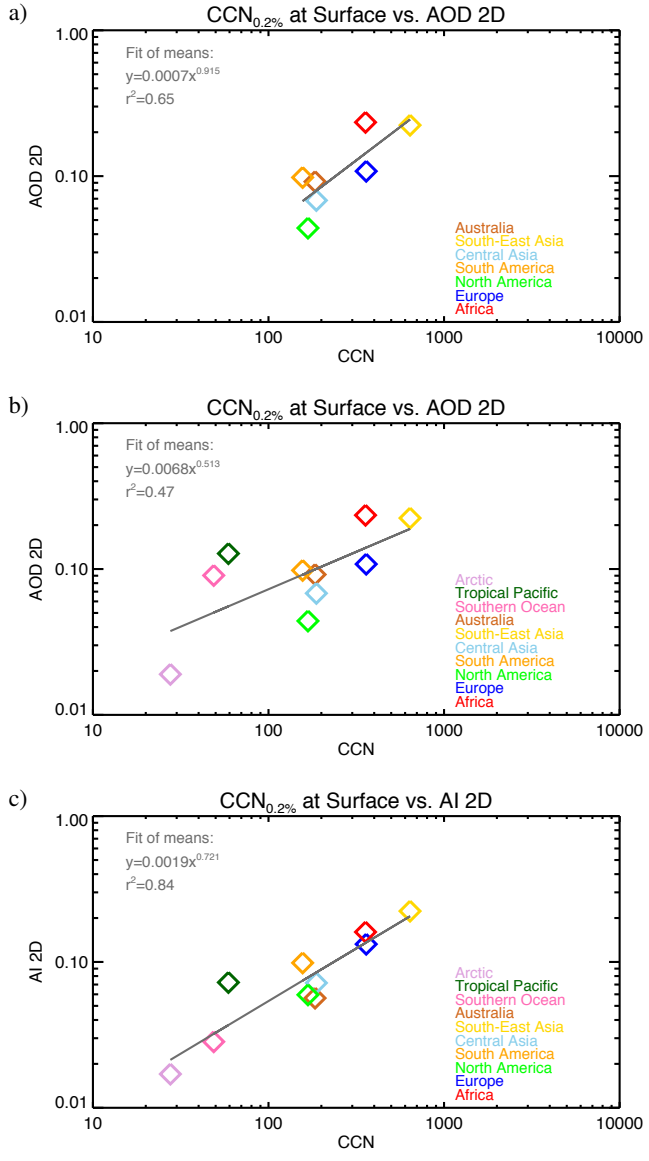

Figure 4. **(a)** Annual continental mean ECHAM-HAM simulated AOD [1] as function of $CCN_{0.2\%}$ [cm^{-3}] and their fit derived from linear regression (gray), **(b)** as **(a)** but including three ocean regions, **(c)** annual continental mean simulated AI as function of $CCN_{0.2\%}$ for continental and ocean regions as in **(b)**; Regional colour coding as in Fig. 3.

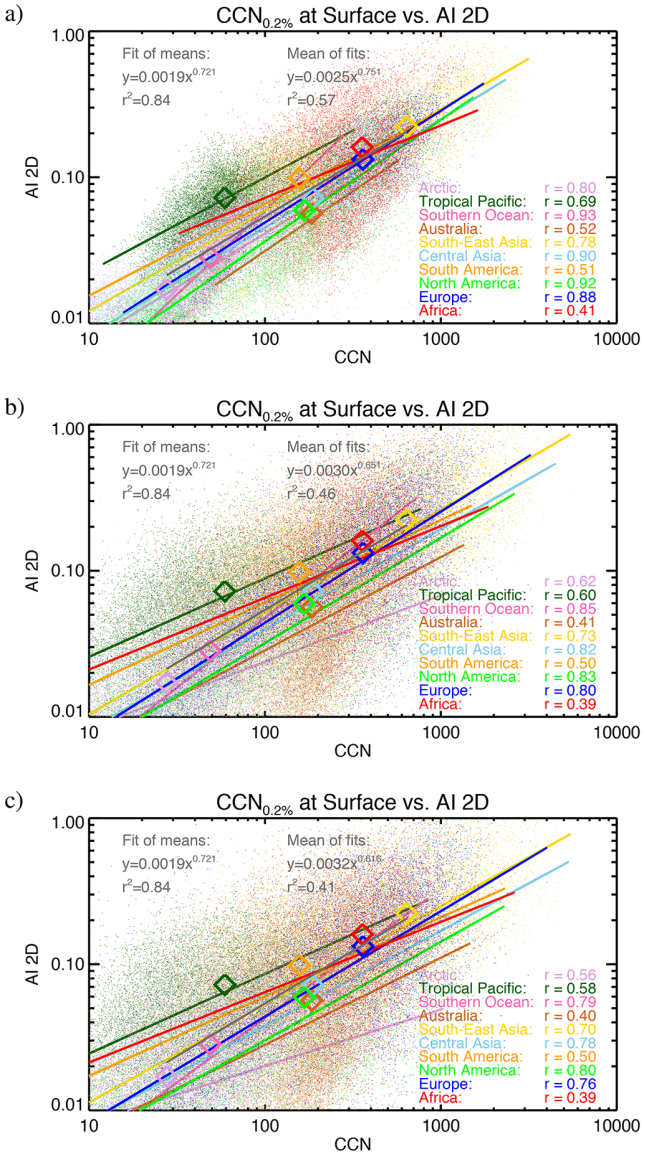

Figure 5. Annual continental mean ECHAM-HAM simulated AI [1] as function of $CCN_{0.2\%}$ [cm^{-3}] (symbols) and their fit derived from linear regression (gray); overlay of **(a)** montly mean, **(b)** daily mean and **(c)** instantaneous 6 hourly pairs of AI and $CCN_{0.2\%}$ (scatter) and their fit derived from linear regression. For visualisation, data in scatterplot randomly sub-sampled to 10 000 pairs. Regional colour coding as in Fig. 3.

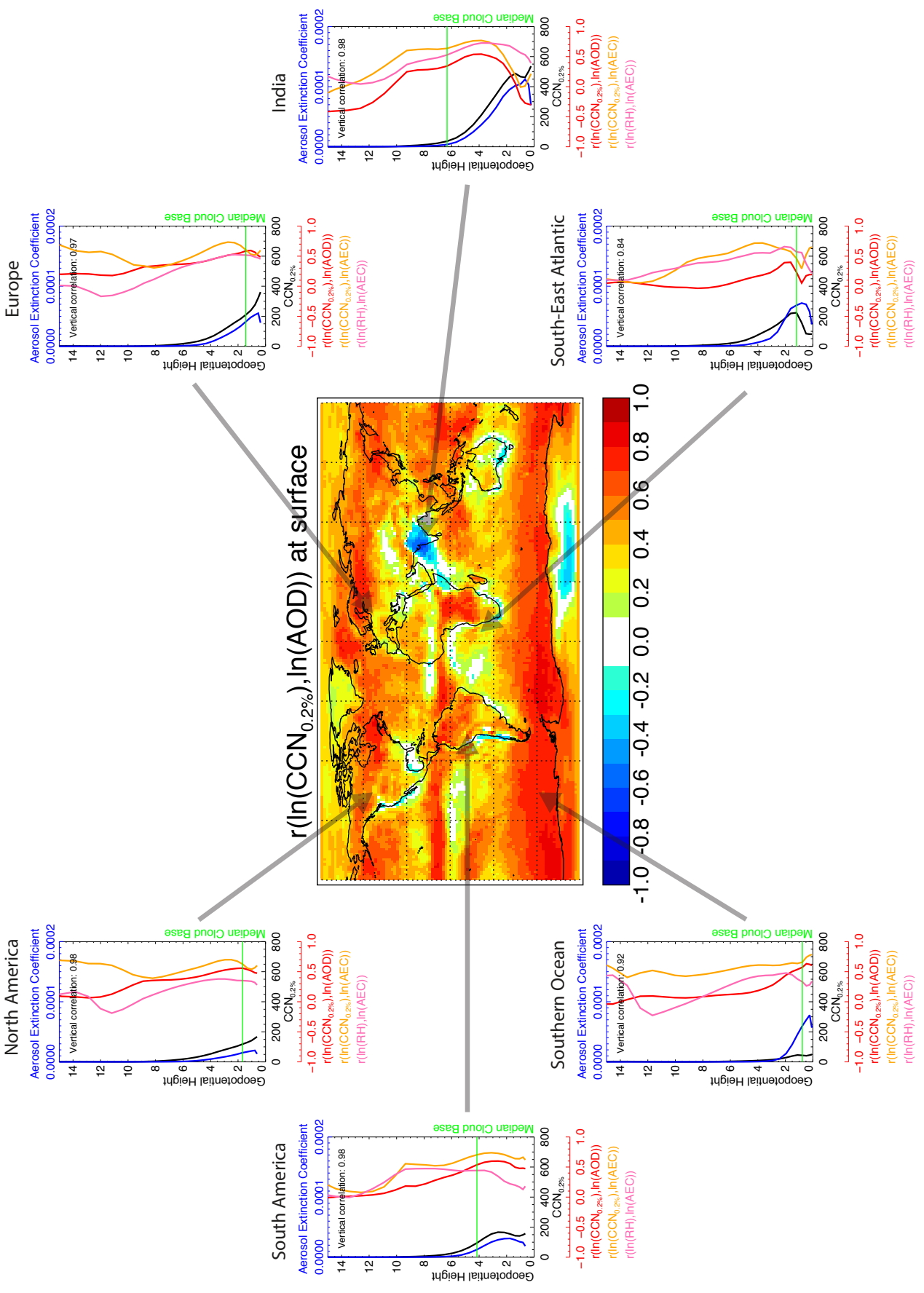

Figure 6. Map of Pearson's correlation coefficient r of ECHAM-HAM simulated surface $\ln(CCN_{0.2\%})$ with column integrated aerosol optical depth $\ln(AOD)$ calculated for each model grid box from one year of 6 hourly pairs. Annual-mean vertical profiles of $CCN_{0.2\%}$ [cm^{-3}] (black), aerosol extinction coefficient (AEC) [m^{-1}] (blue), profile of temporal correlation of $\ln(CCN_{0.2\%})$ with column integrated $\ln(AOD)$ (red), profile of temporal correlation of$\ln(CCN_{0.2\%})$ with vertically resolved extinction coefficient $\ln(AEC)$ orange) and temporal correlation of $\ln(RH)$ with vertically resolved extinction coefficient $\ln(AEC)$ (pink). Also shown is the model median stratiform cloud base for each region (green) – note that this corresponds to the lowest detrainment level in regions dominated by convection, such as India. Regions defined as in Fig. 3.

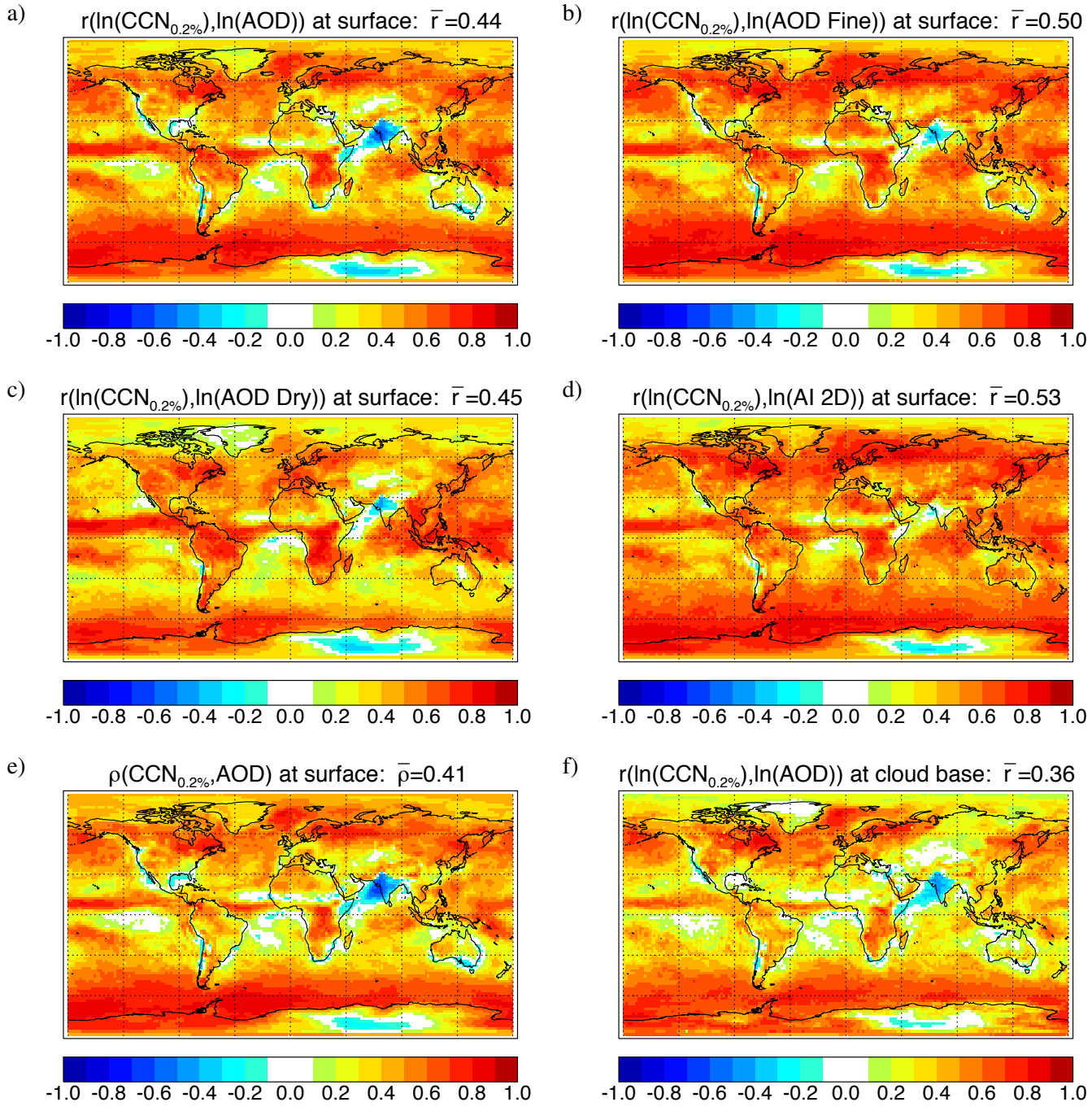

Figure 7. Map of Pearson's correlation coefficient of ECHAM-HAM simulated $CCN_{0.2\%}$ with aerosol radiative properties for **(a)** surface $CCN_{0.2\%}$ with vertically integrated aerosol optical depth, **(b)** surface $CCN_{0.2\%}$ with vertically integrated fine mode aerosol optical depth, **(c)** surface $CCN_{0.2\%}$ with vertically integrated dry aerosol optical depth, **(d)** surface $CCN_{0.2\%}$ with vertically integrated AI, **(e)** Spearman's rank correlation coefficient for surface $CCN_{0.2\%}$ with vertically integrated AOD and **(f)** Pearson's correlation coefficient of $CCN_{0.2\%}$ sampled at cloud base with vertically integrated AOD. Global-mean correlation coefficients are given in the title of each plot.

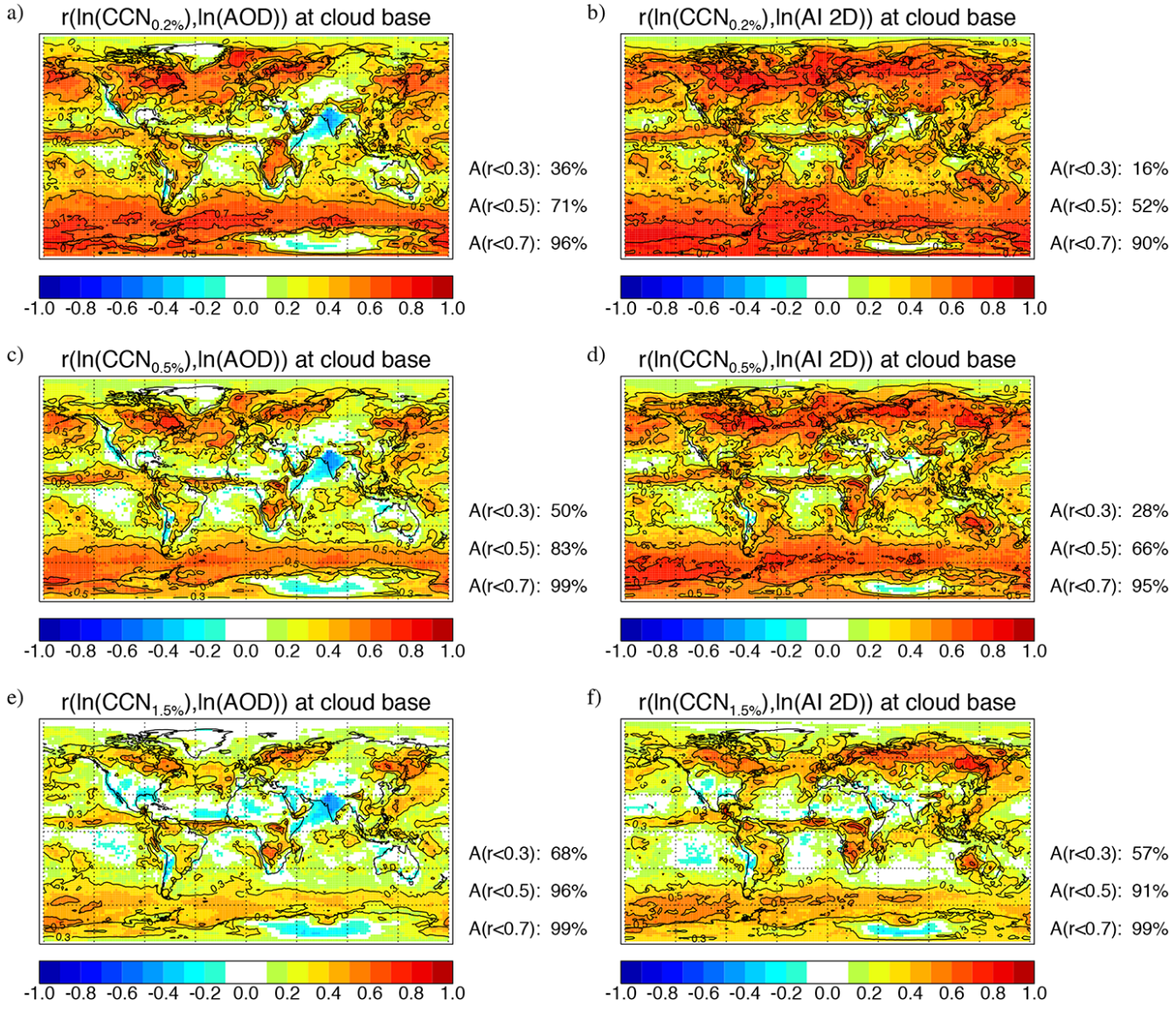

Figure 8. Map of Pearson's correlation coefficient of ECHAM-HAM simulated cloud base CCN with aerosol radiative properties for **(a)** $CCN_{0.2\%}$ with vertically integrated aerosol optical depth, **(b)** $CCN_{0.2\%}$ with vertically integrated aerosol index, **(c)** $CCN_{0.5\%}$ with vertically integrated aerosol optical depth, **(d)** $CCN_{0.5\%}$ with vertically integrated aerosol index, **(e)** $CCN_{1.5\%}$ with vertically integrated aerosol optical depth and **(f)** $CCN_{1.5\%}$ with vertically integrated aerosol index. Fractional area (A) of the globe with $r < 0.3, 0.5, 0.7$.

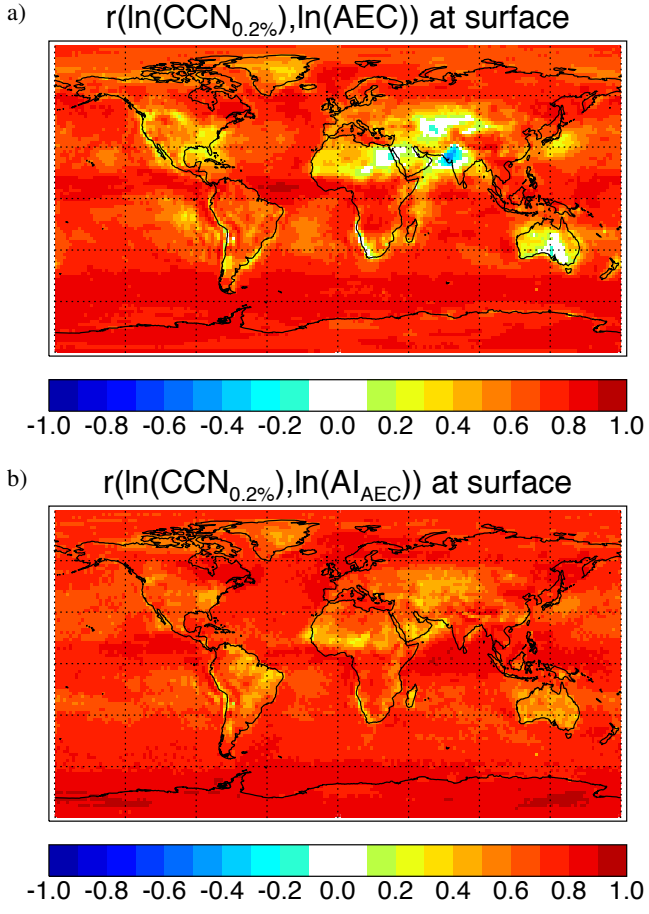

Figure 9. Map of Pearson's correlation coefficient of ECHAM-HAM simulated CCN with vertically resolved aerosol radiative properties: **(a)** surface $\ln(\mathrm{CCN}_{0.2\%})$ with surface $\ln(\mathrm{AEC})$ and **(b)** surface $\ln(\mathrm{CCN}_{0.2\%})$ with surface $\ln(\mathrm{AEC\text{-}AI})$ calculated for each model grid box from one year of 6 hourly pairs.

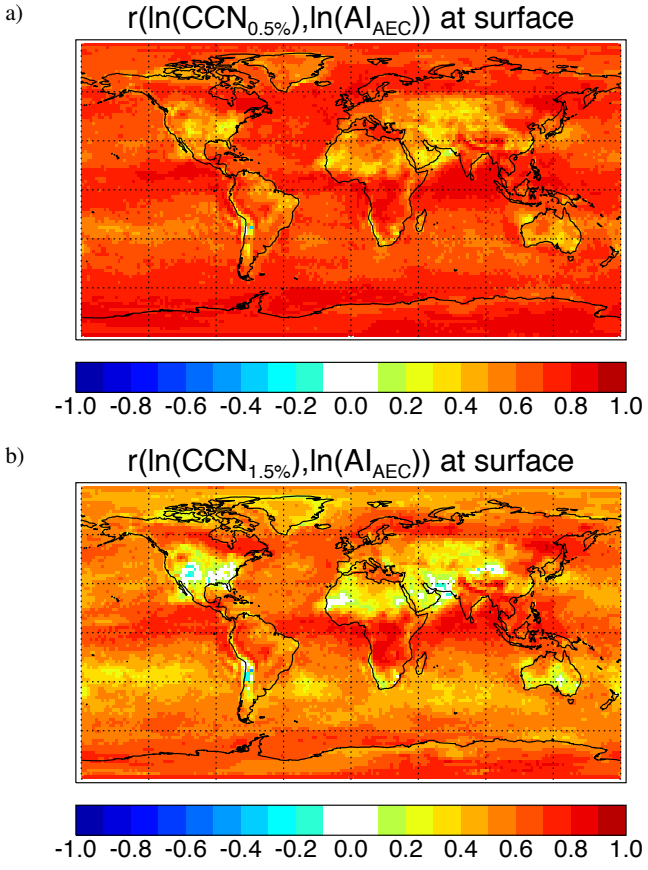

Figure 10. Map of Pearson's correlation coefficient of ECHAM-HAM simulated surface layer $\ln(\mathrm{AI_{AEC}})$ with $\ln(\mathrm{CCN})$ at higher supersaturations: **(a)** $\mathrm{CCN}_{0.5\%}$, **(b)** $\mathrm{CCN}_{1.5\%}$.